

# Optical manipulation of magnetism in spin-charge coupled correlated electron system

Jun Ohara<sup>1,2</sup>, Yu Kanamori<sup>1</sup>, and Sumio Ishihara<sup>1,2</sup>

<sup>1</sup>*Department of Physics, Tohoku University, Sendai 980-8578, Japan and*

<sup>2</sup>*Core Research for Evolutional Science and Technology (CREST), Sendai 980-8578, Japan*

(Dated: March 2, 2013)

Photoirradiation effects in correlated electrons coupled with localized spins are studied based on the extended double-exchange model. In particular, we examine melting of an antiferromagnetic (AFM) charge order insulating state by varying the light intensity. When intense light is irradiated, the AFM insulating characteristics are strengthened, rather than change into the ferromagnetic metallic characteristic, which are expected from the conventional double exchange interaction when carriers are introduced by weak light irradiation or chemical doping. This provides a new principle for optically manipulating magnetism.

PACS numbers: 78.47.J-, 75.78.Jp, 71.30.+h, 71.10.-w

Optical manipulation of magnetism is one of the recent attractive themes in not only condensed matter physics but also modern nano-technologies. Since electron spins do not couple directly to the electric-field component of light, optical control of magnetism has been done in usual by utilizing the circular polarized light through the spin-orbit coupling. This strategy is applied successfully to the controls of magnetism in metallic magnets and some magnetic semiconductors. Another route for the optical control of magnetism is recently developed in correlated electron systems, in which magnetism is strongly coupled with electric transport. There is a possibility to change a magnetic state by modifying the charge state which can be directly controlled by light. One of the advantageous in this manner is a possibility of the ultrafast control of magnetism, since motion of electronic charge is much faster than pure spin motion which is usually governed by the exchange interaction.

Such situation of strong correlation between magnetism and electric transport is realized in a system where local magnetic moments are embedded in a metallic solid. Through the Hund's rule coupling between the local moments and the conduction electrons, the ferromagnetic (FM) double-exchange (DE) interaction operates between the spatially separated local moments [1, 2]. Materials in which the DE interaction gives rise to metallic ferromagnetism include magnetic semiconductors [3, 4], colossal-magnetoresistive (CMR) manganites [5, 6], and so on. The essential aspect of the DE interaction is the kinetic-energy gain of conducting carriers; when local magnetic moments are parallel, electrons can hop between sites without reducing the Hund's rule coupling energy.

A FM metal originating from the DE interaction often competes with other electronic phases. In particular, competition between a FM metal and a charge-ordered (CO) antiferromagnetic (AFM) insulator is widely acknowledged to be the source of the CMR effects in perovskite manganites [6]. A CO AFM insulator is characterized by an energy gap due to the Coulomb interaction

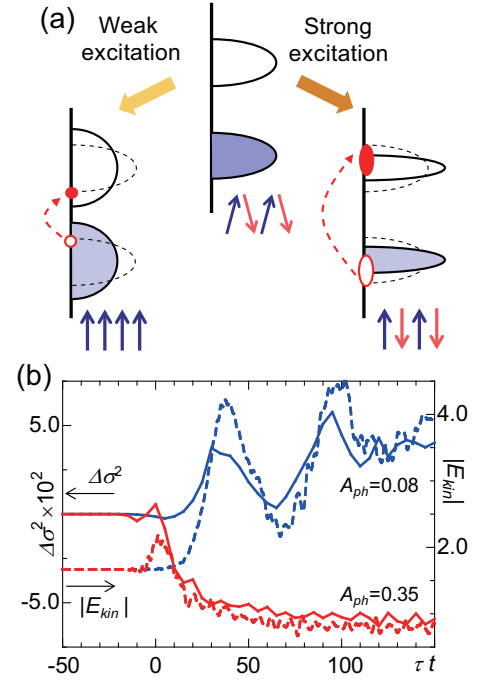


FIG. 1: (color online) (a): Schematic diagram of changes in the electronic density-of-state (DOS) and magnetic structure on weak and strong photon excitations. Bold arrows represent localized spins. Broken arrows imply electronic excitations due to photoirradiation. (b): Changes in the band width  $\Delta\sigma^2$  (bold lines) and the absolute value of the kinetic energy  $E_{kin}$  (broken lines) as functions of time. Blue and red curves are the results for weak pumping ( $A_{ph} = 0.08$ ) and strong pumping ( $A_{ph} = 0.35$ ), respectively. A sign of  $E_{kin}$  is negative, and increasing (decreasing) of  $|E_{kin}|$  implies that carriers gain (loss) the kinetic energy.

and an alternating spin alignment by the AFM exchange interaction. Hole doping by chemical substitution of a CO AFM insulator induces metallic conduction with a FM spin alignment. Many recent experimental and theoretical studies [7–11] have revealed that these correlated changes in magnetism and conduction are also realized

by photo-doping that introduces carriers by optical laser pulses, as shown in the left of Fig. 1(a). This is a naive extension of the DE interaction to excited states, since photon pumping has been widely recognized to convert insulators to metals in a number of organic salts [12, 13], transition-metal oxides [14, 15] and other correlated electron systems [16–19].

In this Letter, we demonstrate that this conventional mechanism for the DE interaction does not operate in highly photoexcited states. As shown in Fig. 1(b), when intense light irradiation introduces carriers to an AFM insulator, the AFM insulating characteristics are strengthened, rather than change into the FM metallic characteristic, which are expected when it is irradiated by weak light. This provides a new principle for optically manipulating magnetism and conducting properties based on varying the light intensity.

To examine changes in magnetism and conduction due to intense light irradiation, we adopt the extended DE model in which mobile electrons couples with local spins through FM Hund's rule coupling  $J_H$ . The explicit Hamiltonian is given by

$$\begin{aligned} \mathcal{H}_0 = & -t \sum_{\langle ij \rangle, \sigma} (c_{i\sigma}^\dagger c_{j\sigma} + H.c.) - J_H \sum_i \mathbf{s}_i \cdot \mathbf{S}_i \\ & + J \sum_{\langle ij \rangle} \mathbf{S}_i \cdot \mathbf{S}_j + V \sum_{\langle ij \rangle} n_i n_j, \end{aligned} \quad (1)$$

where  $c_{i\sigma}$  is the annihilation operator for an electron at site  $i$  and spin  $\sigma (= \uparrow, \downarrow)$ ,  $\mathbf{s}_i (\equiv \sum_{s,s'} c_{is}^\dagger \sigma_{ss'} c_{is'})$  and  $n_i (\equiv \sum_{\sigma} n_{i\sigma} = \sum_{\sigma} c_{i\sigma}^\dagger c_{i\sigma})$  are respectively the spin and charge operators for electrons, and  $\mathbf{S}_i$  is the local spin operator. We restrict the present case to quarter-filling so that the average number of mobile-electrons per site is 0.5. The first two terms correspond to the standard DE Hamiltonian which favors a FM metal. The competing phase, a CO AFM insulator, is stabilized by the Coulomb interaction between nearest neighbor (NN) sites,  $V$ , and the AFM exchange interaction between NN local spins,  $J$ . In the limit of strong Hund's rule coupling,  $J_H \gg t$ , an electron spin and a local spin at the same site are always parallel. This is performed by introducing the local SU(2) gauge transformation, and spin-less fermions,  $\tilde{c}_i$ . Then, the original Hamiltonian is reduced to the following spin-less fermion model:

$$\mathcal{H} = \sum_{\langle ij \rangle} \left( -\tilde{t}_{ij} \tilde{c}_i^\dagger \tilde{c}_j + H.c. + V \tilde{n}_i \tilde{n}_j + J \mathbf{S}_i \cdot \mathbf{S}_j \right), \quad (2)$$

where  $\tilde{n}_i = \tilde{c}_i^\dagger \tilde{c}_i$  is the number of spin-less fermions, and the effective hopping amplitude for fermions depends on the angle of the local spins as  $\tilde{t}_{ij} = t \{ e^{i(\phi_i - \phi_j)/2} \cos(\theta_i/2) \cos(\theta_j/2) + e^{-i(\phi_i - \phi_j)/2} \sin(\theta_i/2) \sin(\theta_j/2) \}$ , as known in Ref. 2.

The pump photon is introduced into the fermion hopping amplitude as the Peierls phase as  $\tilde{t}_{ij} \rightarrow$

$\tilde{t}_{ij} e^{-i \int_{x_i}^{x_j} \mathbf{A}(\tau) \cdot d\mathbf{r}}$  where  $\mathbf{A}(\tau)$  is the vector potential for the pump photon at time  $\tau$ , and  $x_i$  is a position of a site  $i$ . The damped oscillator form is assumed for  $\mathbf{A}(\tau)$  as  $\mathbf{A}(\tau) = A_{ph} \hat{\mathbf{e}} e^{-\gamma_0^2 \tau^2} \cos \omega_{ph} \tau$  with an amplitude  $A_{ph}$ , a damping factor  $\gamma_0 = 0.1t$ , a photon frequency  $\omega_{ph}$ , and a unit polarization vector  $\hat{\mathbf{e}}$ . The time origin is taken to be the center of the photon pulse. The pump photon intensity is expressed by a dimensionless vector-potential amplitude  $A_{ph}$  in terms of the light velocity, the Planck constant and the lattice constant. Impact by the photon irradiation is measured by an "effective" photon density,  $n_{ph} = [E(\tau \gg 0) - E(\tau \ll 0)] / (N \omega_{ph})$ , where  $E(\tau)$  is the electronic energy at time  $\tau$ , and  $N$  is the total number of sites. The present values for the effective density,  $0 \leq n_{ph} \leq 0.15$  for  $0 \leq A_{ph} \leq 0.35$ , are realistic in the usual optical pump-probe experiments [20].

The initial-state electronic structure, time evolution, and excitation spectra are calculated by the numerical exact-diagonalization method in finite size clusters. The one-dimensional  $N (\leq 25)$  site chains and the two-dimensional  $N (= 3 \times 5 \text{ and } 5 \times 5)$  site clusters with the open-boundary condition are adopted. The mobile electron number is taken to be  $N_{ele} = (N + 1)/2$  which corresponds to the quarter filling in the case of the open boundary condition. The time evolution for the electronic wave function,  $|\psi(\tau)\rangle$ , is obtained by solving numerically the time-dependent Schrödinger equation  $i \frac{d|\psi(\tau)\rangle}{d\tau} = \mathcal{H}|\psi(\tau)\rangle$ , based on the Lanczos method [21]. As for the local spin sector, we introduce the classical equations of motion given by  $\frac{d}{d\tau} \frac{\partial \mathcal{L}}{\partial \phi_i} - \frac{\partial \mathcal{L}}{\partial \phi_i} = 0$  and  $\frac{d}{d\tau} \frac{\partial \mathcal{L}}{\partial \theta_i} - \frac{\partial \mathcal{L}}{\partial \theta_i} = 0$ , where  $\mathcal{L}$  is the Lagrangian defined by  $\mathcal{L} = S \sum_i \cos \theta_i \dot{\phi}_i - \langle \mathcal{H} \rangle$  [22], and  $\langle \dots \rangle$  represents the average in terms of the wave function at time  $\tau$ . For simplicity, magnitude of spin is assumed to be  $S = 1/2$ . The equations of motion are solved numerically by utilizing the fourth order Runge-Kutta method.

The ground-state phase diagram almost reproduces the previous results where the extended DE Hamiltonian is analyzed by the density-matrix renormalization-group (DMRG) method [23, 24]. We chose, as an initial state of photo-irradiation processes, the spin-canted CO insulating phase which is located around a boundary between the CO-AFM insulating and FM metallic phases. The photon frequency  $\omega_{ph}$  is tuned to the insulating gap energy (see Fig.4).

Real-time spin- and charge-dynamics after photon-pumping were respectively monitored by the correlation function between the NN localized spins,  $K_S = N_B^{-1} S^{-2} \sum_{\langle ij \rangle} \mathbf{S}_i \cdot \mathbf{S}_j$ , and that between NN mobile charges,  $K_N = N_B^{-1} \sum_{\langle ij \rangle} \langle \tilde{n}_i \tilde{n}_j \rangle$ , where  $N_B$  is the total number of NN bonds. Time evolutions of  $K_S(\tau)$  and  $K_N(\tau)$  for several photon amplitudes calculated in a  $N = 15$  chain are shown in Figs. 2(a) and 2(b). The elapsed time  $\tau$  is denoted in units of  $t^{-1}$ ; it is a few

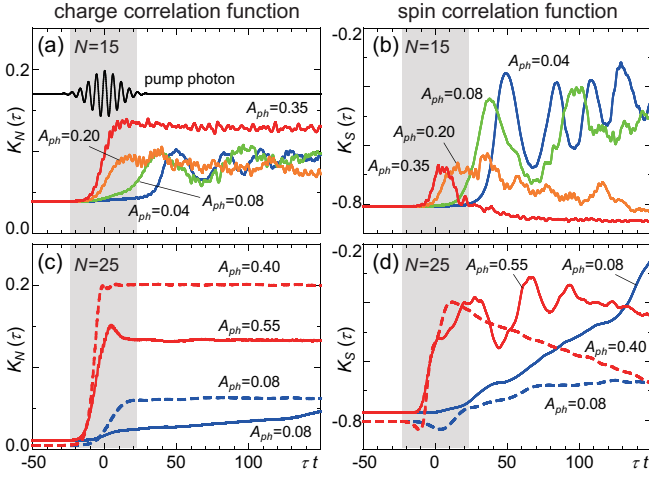


FIG. 2: (color online): Time profiles of the NN charge correlation function  $K_N$ , and those of NN spin correlation function  $K_S$  for several pump-photon amplitudes. Results for the  $N = 15$  chain cluster where  $V/t=1.4$  and  $J/t=1.24$  are shown in (a) and (b). The pump-photon profile with  $\omega_{ph} = 1.1t$  is also shown, and photon amplitudes are  $A_{ph} = 0.04, 0.08, 0.2, 0.35$ . Results for the  $N = 25$  chain (solid lines:  $V/t = 3.1, J/t = 0.625$ ) and  $N = 25$  square (broken lines:  $V/t = 2.1, J/t = 0.31$ ) clusters are shown in (c) and (d). Pump photon energies are chosen to be  $2.7t$  and  $6.2t$  for the chain and square clusters, respectively. Shaded areas represent the time when the pump photons are irradiated.

femto-seconds for conventional transition-metal oxides. In an ideal CO-AFM insulator, we have  $K_N = 0$  and  $K_S = -1$ . The increase in  $K_N$  with  $A_{ph}$  implies that the initial coherent CO collapses on irradiation. In contrast, the time profiles for  $K_S$  are rather complex. For weak pumping ( $A_{ph} \lesssim 0.08$ ), the AFM correlations gradually weaken, and exhibit oscillating behavior. This oscillation might be attributed to the Rabi oscillation between the photoexcited states where energy separations are governed by the effective transfer,  $\tilde{t}_{ij}$ . These profiles in  $K_S$  are well understood from the conventional DE mechanism [10, 25], which is often applied to chemically-doped manganites and weakly photodoped manganites. In contrast, for strong pumping ( $0.2 \lesssim A_{ph}$ ), the AFM correlations suddenly weaken after photon pumping, and gradually recover to the initial AFM state. After  $\tau t \sim 35$ , the AFM correlation is slightly stronger than its initial value. In other words, for  $K_S$  when  $\tau t \gtrsim 35$ , fewer photons collapse the AFM correlation more effectively. These characteristic features in  $K_S(\tau)$  and  $K_N(\tau)$  presented are robust by changing the clusters, as shown in Figs. 2(c) and 2(d). Hereafter, we focus on the dynamics in the  $N = 15$  chain cluster to avoid redundancy and complexity.

To investigate change in the carrier motion predicted by the conventional DE mechanism, Fig. 1(b) shows time profiles for the kinetic energy of the mobile carriers,  $E_{kin} \equiv \langle -\sum_{\langle ij \rangle} \tilde{t}_{ij} \tilde{c}_i^\dagger \tilde{c}_j + H.c. \rangle$  (see broken lines). For

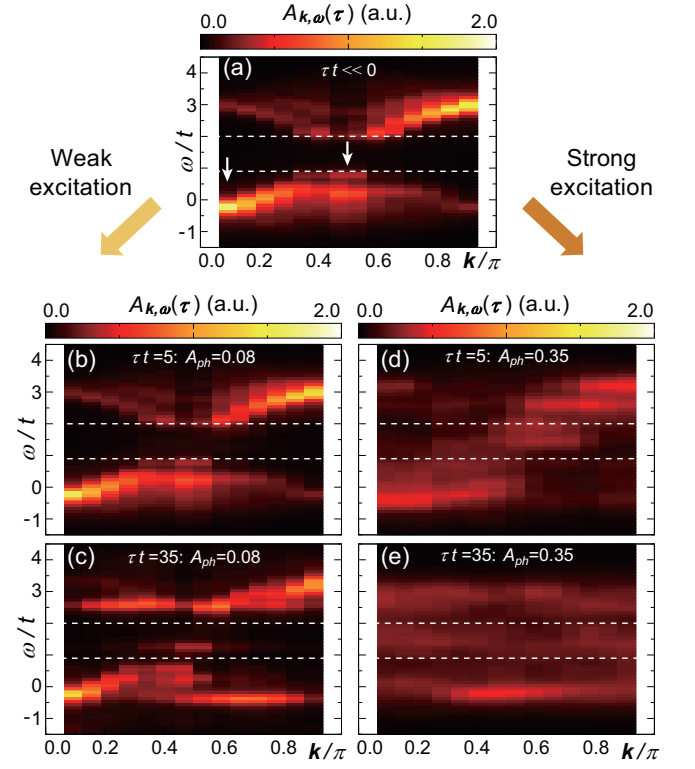


FIG. 3: (color online) Contour plots of one-particle excitation spectra in the momentum-energy space. (a) Results for the initial CO-AFM insulator at  $\tau t \ll 0$ . White arrows denote the top and bottom of the valence band. (b)-(c) The spectra after weak photon pumping ( $A_{ph} = 0.08$ ), and (d)-(e) the spectra after strong photon pumping ( $A_{ph} = 0.35$ ) at  $\tau t = 5$  and  $35$ . White broken lines represent the top of the valence band and the bottom of the conduction band in the initial insulating state. We note that transient spectra in the region of  $|\omega - 1.4t| < \tau^{-1}$  are not meaningful because of the uncertainly principle between time and energy.

weak pumping ( $A_{ph} = 0.08$ ),  $|E_{kin}|$  increases accompanied with oscillations, as expected from the DE mechanism. Completely different behavior is observed for strong pumping ( $A_{ph} = 0.35$ ):  $|E_{kin}|$  decreases monotonically after pumping. These results indicate that this highly excited state is a charge-disordered AFM insulator. Since the total energy is conserved in the simulation, the kinetic-energy gain for weak pumping is compensated by a loss in the AFM exchange-energy of the local spins. In contrast, for strong pumping, reductions in the kinetic and Coulomb energies are compensated by gain in the AFM exchange-energy due to reinforcement of the AFM correlation.

Time- and momentum-resolved electronic structures provide insights into what triggers these unusual highly photoexcited states. Transient correlated electronic bands are monitored by time-dependent one-particle excitation spectra, i.e. time-resolved (inverse) photoemission spectra (PES).

This is divided by the electronic part defined by  $A_{\mathbf{k},\omega}^e(\tau) = -\pi^{-1}\text{Im}\sum_{nml}\psi_n^*(\tau)(\tilde{c}_{\mathbf{k}}^\dagger)_{nm}(\tilde{c}_{\mathbf{k}})_{ml}\psi_l(\tau)(-\omega - E_m + E_n + i\eta)^{-1}$ , and the hole part by  $A_{\mathbf{k},\omega}^h(\tau) = -\pi^{-1}\text{Im}\sum_{nml}\psi_n^*(\tau)(\tilde{c}_{\mathbf{k}})_{nm}(\tilde{c}_{\mathbf{k}}^\dagger)_{ml}\psi_l(\tau)(\omega - E_m + E_l + i\eta)^{-1}$ , where we introduce the energy eigen value  $E_m$ , the eigen state  $|m\rangle$ ,  $(\tilde{c}_{\mathbf{k}})_{nm} = \langle n|\tilde{c}_{\mathbf{k}}|m\rangle$ ,  $\psi_n(\tau) = \langle n|\psi(\tau)\rangle$ , and an infinitesimal constant  $\eta = 0.1t$ . These formulae are derived based on the linear response theory in the photo-excited transient state [24]. Results for weak and strong pumping are presented in Fig. 3. In the initial CO-AFM insulator (see Fig. 3(a)), a direct gap in the electron energy bands opens at the center of the Brillouin zone, e.g.  $\mathbf{k} = \pi/2$ . After photon-pumping, a large change in the electronic spectra occurs due to many-body effects. For weak pumping at  $A_{ph} = 0.08$  (left panels in Fig. 3), changes in the electronic structure are triggered by the spectral-weight transfer around  $\mathbf{k} = \pi/2$  from the valence band to the in-gap region. Specifically, electrons at the top of the valence band are excited, and a new in-gap state is generated around the same momentum. On the other hand, for strong pumping at  $A_{ph} = 0.35$  (right panels in Fig. 3), the electronic-structure changes across the Brillouin zone. In particular, high spectral weights around the bottom of the valence band ( $\mathbf{k} \simeq 0$ ) in the initial state are smeared out, and are transferred to the initial gap region and the whole valence-band region.

To analyze the transient valence-band width in more detail, we introduce the second moment of the valence band defined by  $\sigma^2(\tau) = N^{-1}\int_{-\infty}^{E_{top}}\sum_{\mathbf{k}}A_{\mathbf{k},\omega}^e(\tau)(\omega - \omega_c)^2d\omega$ , where  $\omega_c$  is the center of the band given by  $\omega_c = \int_{-\infty}^{E_{top}}\sum_{\mathbf{k}}A_{\mathbf{k},\omega}^e(\tau)\omega d\omega / \int_{-\infty}^{E_{top}}\sum_{\mathbf{k}}A_{\mathbf{k},\omega}^e(\tau)d\omega$  and  $E_{top}$  is the energy at the top of the valence band for  $\tau t \ll 0$ . We define the difference from the initial band width as  $\Delta\sigma^2 = \sigma^2(\tau) - \sigma^2(\tau \ll 0)$ . Numerical results in one-dimensional 15 site chain are presented in Fig. 1(b). For weak pumping ( $A_{ph} = 0.08$ ),  $\Delta\sigma^2$  increases and shows positive values, as expected from the conventional DE scenario. On the other hand, results are completely different for strong pumping ( $A_{ph} = 0.35$ ). That is, the band width becomes wide (narrow) for weak (strong) pumping. These are the similar behaviors with the changes in the kinetic energy  $E_{kin}$ , explained previously.

We now present a physical picture for the highly photoexcited state (see Fig. 1(a)). For weak pumping, as shown in Figs. 3(b) and 3(c), holes are generated near the top of the valence band. This situation is similar to the state induced by chemical doping of holes. According to the conventional DE mechanism, a broadening of the valence band accompanied with the FM alignment of local spins occurs in order to gain the hole kinetic-energy. However, for strong pumping, as shown in Figs. 3(d) and 3(e), many photodoped holes are introduced near the bottom of the band. The band narrowing increases the

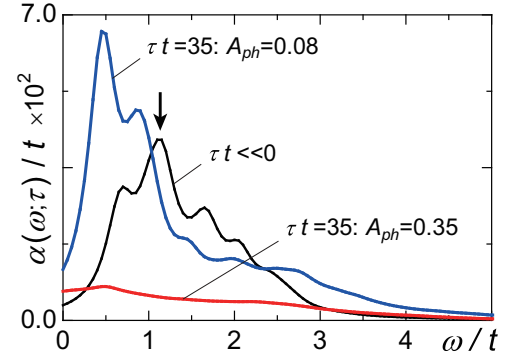


FIG. 4: (color online): Photoabsorption spectra after weak photon pumping ( $A_{ph} = 0.08$ , a blue line) and strong photon pumping ( $A_{ph} = 0.35$ , a red line) at time  $\tau t = 35$ . Absorption spectra for the initial CO-AFM insulator are also shown by a black line. Bold arrow indicates the pump photon energy  $\omega_{ph} = 1.1t$  which is a peak energy of the optical absorption spectra in the initial state. We note that transient spectra in the region of  $|\omega| < 0.03t$  are not meaningful because of the uncertainly principle between time and energy.

hole kinetic-energy gain. This is considered to be the origin of the enhanced AF insulator characteristics induced by strong photon pumping.

We propose that time-resolved pump-probe experiments can confirm the present unusual photoexcited state. The pump-probe optical absorption spectra is calculated by the linear response theory for the probe photon defined by  $\alpha(\omega; \tau) = -\pi^{-1}\text{Im}\langle \mathcal{J}(\omega - \mathcal{H} + \langle \mathcal{H} \rangle + i\eta)^{-1} \mathcal{J} \rangle$ , where we introduce the current operator given by  $\mathcal{J} = -i\sum_{\langle ij \rangle} \tilde{t}_{ij} \tilde{c}_i^\dagger \tilde{c}_j + H.c.$  [24]. Figure 4 shows optical pump-probe spectra (the transient optical absorption spectra  $\alpha(\omega; \tau)$ ) at time  $\tau t = 35$ . A gap-like feature is observed in  $\alpha(\omega; \tau)$  for an initial CO insulator. A low-energy peak grows in the initial optical gap for  $A_{ph} = 0.08$ , as expected for the metallic state. On the other hand, the reduction in the whole spectral intensity in  $A_{ph} = 0.35$  implies enhancement of the localized character of mobile carriers. The low spectral intensity in the initial gapped region for strong pumping indicates collapse of the coherent CO state.

The present study reveals a new aspect of the DE system. The reinforcement of the AFM correlation and the band narrowing observed in the present study were not expected for chemical doping and thermal carrier creation. These phenomena are only realized in photoirradiated spin-charge coupled systems for which high electronic excitation is possible at high photon densities, and the band width is directly controlled by the spin configurations. Thus, the strongly pumped state is identified as a photo-induced hidden state, which will be directly detected by recently developed time-resolved resonant x-ray diffraction and angular resolved PES. The clear difference between weak and strong pumping provides a possible means for optically manipulating magnetism



and conduction based on photon intensity. After several-hundred femto seconds, which is beyond the limits of the present simulation, spin relaxation originating from the spin-orbit interaction begins to occur and it tends to stabilize the FM metal. Energy relaxation will eventually restore the system to the initial CO-AFM insulating state. In other words, relaxation effects for both angular momentum and energy relax the system to trivial fixed points. The unique photo-induced phenomena occur in early stages before relaxation starts to operate.

We thank H. Matsueda, S. Koshihara, S. Iwai, and Y. Okimoto for helpful discussions. This work was supported in part by Grant-in-Aid for Scientific Research Priority Area from the Ministry of Education, Science and Culture of Japan. Some of the numerical calculations were performed using the supercomputing facilities at ISSP, the University of Tokyo, and Kyoto University.

- 
- [1] C. Zener, Phys. Rev. **82**, 403 (1951).
  - [2] P. W. Anderson and H. Hasegawa, Phys. Rev. **100**, 675 (1955).
  - [3] H. Munekata *et al.*, Phys. Rev. Lett. **63**, 1849 (1989).
  - [4] T. Dietl *et al.*, Science **287**, 1019 (2000).
  - [5] E. Dagotto, New J. Phys. **7**, 67 (2005).

- [6] Y. Tokura, Rep. Prog. Phys. **69**, 797 (2006).
- [7] M. Fiebig *et al.*, Science **280**, 1925 (1998).
- [8] X. J. Liu *et al.*, Phys. Rev. B **64**, 100401(R) (2001).
- [9] H. Ehrke *et al.*, Phys. Rev. Lett. **106**, 217401 (2011).
- [10] H. Matsueda and S. Ishihara, J. Phys. Soc. Jpn. **76**, 083703 (2007).
- [11] W. Koshihara, N. Furukawa, and N. Nagaosa, Phys. Rev. Lett. **103**, 266402 (2009).
- [12] Y. Kawakami *et al.*, Phys. Rev. Lett. **105**, 246402 (2010).
- [13] M. Chollet *et al.*, Science **307**, 86 (2005).
- [14] A. Cavalleri *et al.*, Phys. Rev. Lett. **87**, 237401 (2001).
- [15] H. Okamoto *et al.*, Phys. Rev. B **83**, 125102 (2011).
- [16] O. P. Matveev *et al.*, Phys. Rev. B **77**, 035102 (2008).
- [17] N. Tsuji, T. Oka, and H. Aoki, Phys. Rev. Lett. **103**, 047403 (2009).
- [18] B. Moritz, T. P. Devereaux and J. K. Freericks, Phys. Rev. B **81**, 165112 (2010).
- [19] M. Eckstein and P. Werner, Phys. Rev. B **84**, 035122 (2011).
- [20] M. Matsubara *et al.*, Phys. Rev. B **77**, 094410 (2008).
- [21] T. J. Park and J. C. Light, J. Chem. Phys. **85**, 5870 (1986).
- [22] K. Obata and G. Tatara, Phys. Rev. B **77**, 214429 (2008).
- [23] D. J. García *et al.*, Phys. Rev. Lett. **85**, 3720 (2000).
- [24] Y. Kanamori, H. Matsueda, and S. Ishihara, Phys. Rev. B **82**, 115101 (2010).
- [25] Y. Kanamori, H. Matsueda, and S. Ishihara, Phys. Rev. Lett. **103**, 267401 (2009).